AGU PUBLICATIONS

Geophysical Research Letters

RESEARCH LETTER
10.1002/2014GL062180

Key Points:
- New type of Coriolis-balanced circulation in ice-covered lakes is discovered
- The bottom slope plays a key role in acceleration of the of anticyclonic flow
- The only driver is the buoyancy sink along the shore: general for coastal flows

Correspondence to:
G. B. Kirillin,
kirillin@igb-berlin.de

Citation:
Kirillin, G. B., A. L. Forrest, K. E. Graves, A. Fischer, C. Engelhardt, and B. E. Laval (2015), Axisymmetric circulation driven by marginal heating in ice-covered lakes, *Geophys. Res. Lett.*, *42*, 2893–2900, doi:10.1002/2014GL062180.

Received 10 OCT 2014
Accepted 27 MAR 2015
Accepted article online 31 MAR 2015
Published online 21 APR 2015

Axisymmetric circulation driven by marginal heating in ice-covered lakes

G. B. Kirillin[1], A. L. Forrest[2,3], K. E. Graves[4], A. Fischer[5], C. Engelhardt[1], and B. E. Laval[4]

[1]Leibniz-Institute of Freshwater Ecology and Inland Fisheries, Berlin, Germany, [2]Australian Maritime College, University of Tasmania, Launceston, Tasmania, Australia, [3]Tahoe Environmental Research Center, University of California - Davis, Incline Village, Nevada, USA, [4]Department of Civil Engineering, University of British Columbia, Vancouver, British Columbia, Canada, [5]Institute for Marine and Antarctic Studies, University of Tasmania, Launceston, Tasmania, Australia

Abstract Below the temperature of maximum density (TMD) in freshwater lakes, heating at the lateral margins produces gravity currents along the bottom slope, akin to katabatic winds in the atmosphere and currents on continental shelves. We describe axisymmetric basin-scale circulation driven by heat flux at the shorelines in polar Lake Kilpisjärvi. A dense underflow originating near the shore converges toward the lake center, where it produces warm upwelling and return flow across the bulk of lake water column. The return flow, being subject to Coriolis force, creates a lake-wide anticyclonic gyre with velocities of 2–4 cm s^{-1}. While warm underflows are common on ice-covered lakes, the key finding is the basin-scale anticyclonic gyre with warm upwelling in the core. This circulation mechanism provides a key to understanding transport processes in (semi) enclosed basins subject to negative buoyancy flux due to heating (or cooling at temperatures above TMD) at their lateral boundaries.

1. Introduction

Circulation in ice-covered lakes is poorly investigated due to remoteness of the field sites, isolation of the water bodies by the ice cover, and water velocities at the detection limit of conventional instrumentation. A deeper insight into the driving mechanisms of under-ice freshwater circulation has a broad area of application including (i) dynamics of purely buoyancy-driven flows, affected by nonlinear effects, such as freshwater density anomaly [*Farmer*, 1975; *Kirillin and Terzhevik*, 2011]; (ii) transport of heat and dissolved matter in subglacial and proglacial lakes with implications for polar lakes and extraterrestrial water systems [*Siegert*, 2005; *McKay et al*., 2005]; and (iii) ecosystem dynamics of the seasonally ice-covered temperate lakes, where the "rebirth" of the ecosystem after the low productive winter period is triggered by the under-ice transport of nutrients and algae cells over the water column [*Kelley*, 1997; *Golosov et al*., 2007].

In seasonally ice-covered lakes, circulation is primarily forced by (1) release of heat stored in lake sediments during the preceding ice-free season, (2) solar radiation penetrating ice cover, and (3) buoyancy flux resulting from differential heating and surface inflows. The first forcing prevails during the initial stage of the ice-covered period and generates downslope density currents [*Rizk et al*., 2014, and citations therein]. The second forcing mechanism dominates lake circulation in spring, when significant solar radiation penetrates the ice cover, producing vertical convection in the upper water layers [*Mironov et al*., 2002, and citations therein] and initiating secondary circulation through variation in ice thickness and (or) optical properties [*Forrest et al*., 2008]. The third forcing occurs in spring as snow and ice melt in the catchment and on the lake. Seasonal ice melt starts along the shoreline [*Kirillin et al*., 2012] forming ice-free margins, known as moats [*Nolan et al*., 2002]. While formation of moats by lateral heating and surface meltwater runoff is recognized as the main regulator of the biochemical cycle in perennially ice-covered, proglacial Antarctic lakes [*Spigel and Priscu*, 1998], there has been limited investigation of its role in lake circulation [*Salonen et al*., 2014]. The lateral heating is, however, a potential source of strong density-driven currents created by the radiative heating of open water in moats augmented by the heat inflow from the warm surface runoff. The resulting negative buoyancy flux may generate density-driven plunging underflow providing an additional lake-wide circulation driver.

Unlike open water lakes, where surface wind shear usually mixes horizontal density gradients on relatively short time scales, under-ice density flows may persist for up to several months [*Huttula et al*., 2010; *Rizk et al*., 2014]. These longer time scales allow sufficient time for density anomalies to adjust to Coriolis

forcing, without becoming mixed into the background stratification, on length scales less than $O(1\,km)$ as given by the internal Rossby radius of deformation [*Kirillin et al.*, 2012; *Forrest et al.*, 2013]. Hence, circulation in ice-covered lakes larger than the internal Rossby radius is likely a nearly steady state Coriolis-balanced density flow and thus an illuminative analogue of large-scale density flows in the ocean and in the planetary atmospheres [*Rhines*, 1993, 1998].

Below we present the results from a field campaign on polar Lake Kilpisjärvi, northern Fennoscandia. The warm spring in 2013, with air temperatures in May approaching +30°C, preceded by a relatively cold winter, provided strong heat input by melted water and formation of moats at the lake shores, while the bulk of the lake remained isolated from the atmosphere by the 60 cm thick lake ice cover. The cross-lake axial distribution of density and vertical profiles of current velocities suggest this forcing could form a quasi-stationary axisymmetric circulation pattern. We analyze this pattern in terms of the order-of-magnitude balance of the main driving forces, demonstrate its lake-wide steady state character, and discuss the role of the bottom slope balanced by the Coriolis force in the anticyclonic character of the observed circulation.

2. Study Site and Methods

Kilpisjärvi (Figures 1a and 1b) is a midsize (surface area 37 km^2, maximum depth 57 m) polar (69°01′N 20°49′E) lake with an ice-covered period of ~220 days [*Lei et al.*, 2012]. The field campaign was conducted from 25 May to 6 June 2013, when the lake area was exposed to Sun for nearly 24 h daily. The meteorological conditions followed a colder than average winter season (G. Kirillin, 2012/2013 winter ice was ~10 cm thicker than the long-term mean; Finnish Environmental Service, personal communication, 2013). At the start of the campaign, no detectable snow cover was present on the 60 cm thick ice cover. The snow accumulated by surrounding mountains produced meltwater runoff into the lake through the main tributary at the northern tip of the lake and a number of small streams and drainages around the lake. The ice cover edge (Figure 1b) was digitized from WorldView-1 satellite imagery collected on 1 June 2013 except for the lower part of the lake, which, absent in the satellite image, was estimated from field observations (blue dashed line).

Two moored acoustic Doppler current profilers (ADCP) were deployed at two sites along the 20 m isobath (Sites A1, A2 in Figure 1b). An upward-looking 600 kHz ADCP (Teledyne RD Instruments, USA) operated in the "Doppler Mode 1" measured velocity every 120 s at 2–20 m elevation above the lake bottom in 0.3 m bins. Due to a lack of sound reflecting particles in lake water, the acoustic signal from the upper 16–20 m was too weak to reliably estimate velocity. In the bottom boundary layer, a high-resolution HR AQUADOPP (Nortek AS, Norway) measured velocities from 0 to 2 m elevation above the lake bottom in the pulse-to-pulse coherent profiling mode at temporal resolution of 1 s and vertical resolution of 0.02 m.

On 26 May 2013, we completed a 2800 m long conductivity-temperature-depth (CTD) transect along the transverse axis of the lake. Vertical profiles were taken through ice holes made at 50 m horizontal spacing (Figure 1b) by lowering an RBR CTD profiler (Richard Branker Research, Canada; sampling frequency 6 Hz, temperature resolution and accuracy of <0.00005°C and ± 0.002 °C, respectively, and conductivity resolution and accuracy of $<0.02\,\mu S/cm$ and $\pm 3\,\mu S/cm$, respectively). On 27 May 2013 inflow temperatures were measured using RBR CTD profilers at 15 locations where surface inflows were observed along the northeast side of Kilpisjärvi. At each location, the instrument was placed just below the water surface (at ~0.1 m) and taken to be representative of the entire stream. As none of the streams exceeded 0.5 m total water depth, they were assumed to be isothermal.

3. Observations

The CTD transect revealed a nearly axisymmetric temperature distribution across the lake with a warmer upwelling-like water column in the center of the lake and a near-bottom layer of warm water aligned with the bottom slope that thickened toward the lake center (Figure 1d). The temperature distribution was observed to be symmetric about the central vertical axis with colder water between the central upwelling area and the warmer water at the sidewalls of the lake.

A continuous, several-meter-wide moat around the entire lake was either observed or inferred from the WorldView-1 imagery (Figure 1b). Observed temperature of inflowing streams ranged from 4.4 to 15.8°C and an observed mean of 9.5 ± 3.6°C. Smaller creeks were observed to have higher water temperatures.

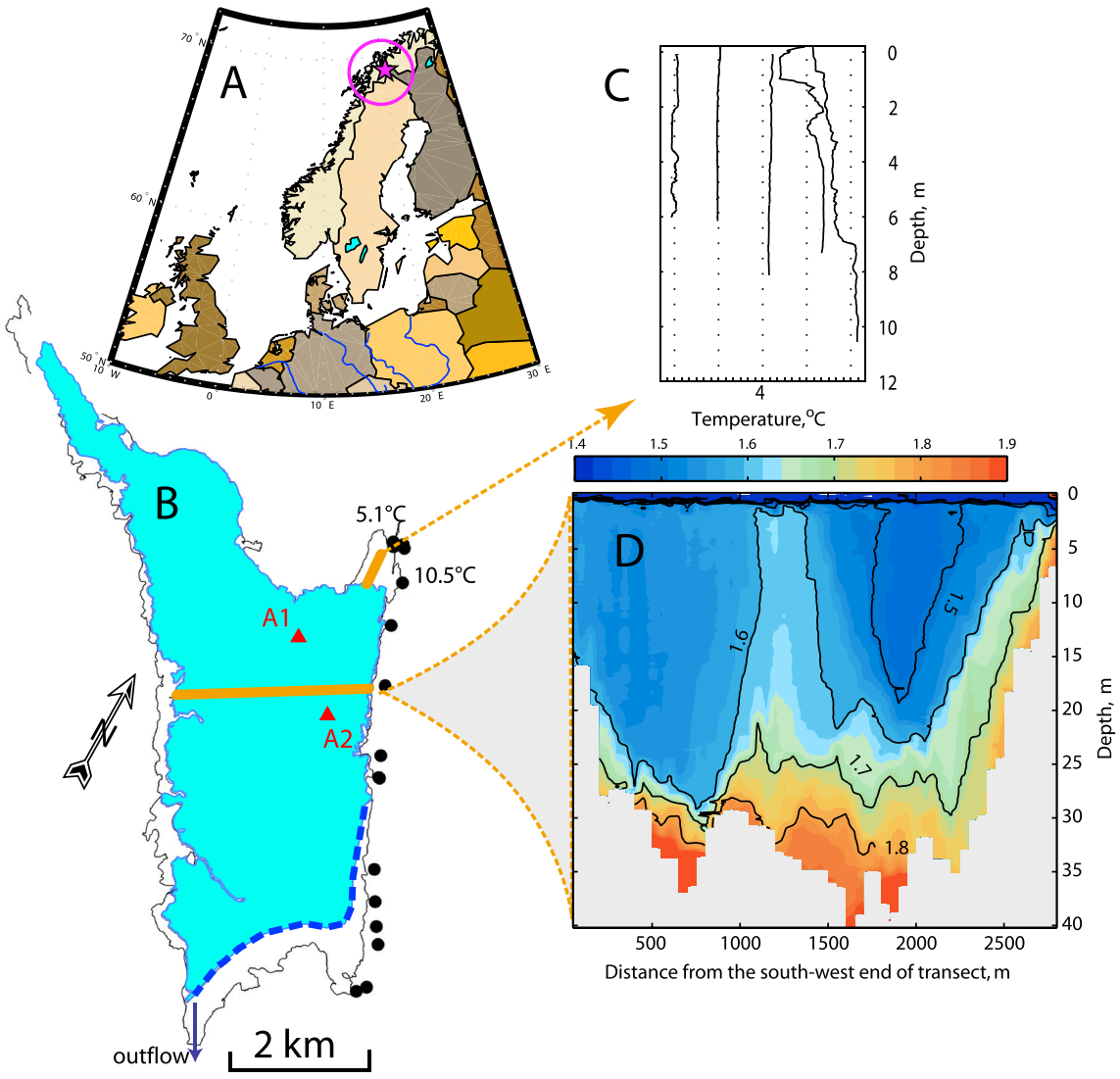

Figure 1. (a) Geographic location and (b) ice cover map of Lake Kilpisjärvi with shoreline (black line), ice cover extent (light-blue area) with dashed line in the southeastern part of the lake delineating the area missing in satellite imagery, positions of the CTD transects (thick yellow lines), and inflowing streams with measured temperatures (black dots), and the current velocity recorders (red triangles). (c) Temperature profiles taken every 150 m in the large northeastern moat fed by the main inflow and a small adjacent creek. Measured temperature of these two inflows are indicated at the corresponding black dots in Figure 1b. Inflow specific conductance was similar to lake water, i.e., ~20 μS cm^{-1}. The leftmost profile is the closest to the lake shore, the rightmost profile is at the ice edge. Profiles are drawn with 1.5°C horizontal offset, and dashed vertical lines correspond to 4°C for each profile. (d) Temperature distribution along the cross-lake transect.

CTD profiles taken in the open water areas reveal a vertically fully mixed water column at temperatures ≥4°C and a horizontal front adjacent to the ice margin with a plunging warm underflow forming within ~200 m distance from the ice margin (Figure 1c). This suggests that the heat input at the lateral margins from warm inflows and differential heating between the open water and the adjacent ice-covered lake combine to create a constant temperature boundary condition close to 4°C at the ice margin. In the following analysis, 4°C will be used as a scale temperature for source water of the underflow.

Velocity measurements in the bulk water column (Figure 2b) indicate quasi-stationary longshore flow with velocity magnitudes of ~2 cm s^{-1} increasing upward. The cross-shore velocity component is weak (<1 cm s^{-1}) and is shoreward in the upper layers turning to offshore and increasing in magnitude in the lower 5 m of the water column. The near-bottom AQUADOPP velocity data support the suggestion of a strong downslope density current here (Figure 2c). The offshore current with magnitudes of 2–4 cm s^{-1} occupies the bulk of the lowest 2 m of the water column with a mean longshore component not

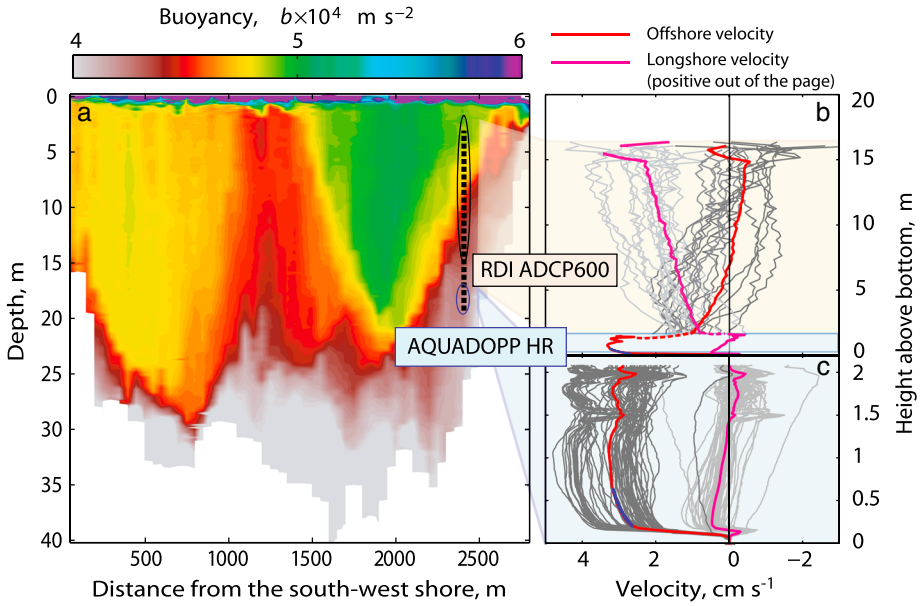

Figure 2. (a) Buoyancy distribution along the CTD transect from Figure 1b; approximate position of the two current velocity recorders relative to the lakeshore and their vertical coverage are marked by the thick dotted line and thin ellipses, respectively. (b) Combined individual (gray lines) and time-averaged (red lines) vertical profiles for the offshore and longshore velocity components collected with the ADCP. (c) Same as preceding panel for the high-resolution AQUADOPP data from the bottom boundary layer. The blue line marks the logarithmic fit of the offshore velocity component.

exceeding 0.5 cm s^{-1}. When combined with the temperature data (Figure 1d), the records suggest a lake-wide circulation pattern with converging density current in the bottom boundary layer and diverging anticyclonic circulation in the upper part of the lake volume coupled through a warm water upwelling in the center of the lake. The vertically uniform flow with velocity magnitudes of 2–4 cm s^{-1} occupying the entire 20 m deep water column at the measurement site is surprisingly strong for a small ice-covered lake [*Rizk et al.*, 2014].

Windless conditions existed during the entire period of observations indicating no wind effects on circulation under ice and in the moats. On 2 June wind speeds increased to ~5 m s^{-1} (data from the nearby weather station), followed by immediate ice breakup.

4. Circulation Characteristics and Driving Mechanisms

We now demonstrate by means of scaling analysis that lateral buoyancy forcing from warm water at the lake periphery (due to the combined effects of differential heating in the moat and warm inflow) together with the Coriolis acceleration is the main force producing the axisymmetric density distribution and the anticyclonic circulation in the bulk of the lake with downslope bottom current beneath. In the following analysis, we make use of buoyancy in its conventional definition $b = -g(\rho - \rho_0)\rho_0^{-1}$, where $g \approx 9.81$ m s^{-1} is gravitational acceleration, ρ is the water density, and ρ_0 is the density value at the temperature of maximum density of freshwater $T_0 \approx 3.98$°C. Density was calculated from temperature following *Chen and Millero* [1986]. The effect of dissolved salts on water density was neglected because specific conductivity is very low (14 to 20 μS cm^{-1}) and nearly homogeneous across the lake.

4.1. Lateral Buoyancy Forcing

The ambient lake temperature was estimated from the mean water temperature excluding upwelling or marginal regions as T_L ~1.7°C. As discussed above, the scale temperature for inflows is taken as $T_0 \approx 4$°C. The negative buoyancy flux associated with the lateral temperature difference, $\Delta T = T_0 - T_L \approx 4\,°C - 1.7\,°C = 2.3°C$ produces a plunging gravity flow along the bottom slope, whose characteristic velocity scale U_{scale} can be estimated as [*Rizk et al.*, 2014, equations (17) and (19)] $U_{scale} = (1/2 g\alpha_T \Delta T^2 L_\beta \sin\beta)^{1/2} = (1/2 g\alpha_T \Delta T^2 H)^{1/2} \sim 10^{-1}$ [m s^{-1}], where

$\alpha_T \approx 1.65 \times 10^{-5}\,K^{-2}$ is the thermal expansion coefficient in the quadratic freshwater equation of state, L_β is the distance along the bottom slope with declination β, and $H \approx 20$–30 m is the water depth at distance L_β. Taken as an upper limit ignoring any frictional forces, this estimate for U_{scale} is in agreement with the mean downslope velocity $u_{down} = 2$–$4\,cm\,s^{-1}$ measured in the bottom 2 m of the water column (Figure 2b). Hence, the buoyancy forcing due to lateral heating is strong enough to be a single driving mechanism for the observed gravity flow along the sloping boundary.

4.2. Negatively Buoyant Plume

The velocity within 0.5–0.6 m above the lake bottom has a nearly logarithmic profile (Figure 2c). The shear velocity $u_* = 1.7 \times 10^{-3}\,m\,s^{-1}$ and roughness length $z_0 = 4 \times 10^{-4}$ m were obtained by fitting the mean velocity profile with the law of the wall. The roughness length z_0 is close to $\nu u_*^{-1} \sim 10^{-3}$ m, suggesting a smooth (viscosity-dominated) boundary flow. The velocity scale U_{scale} gives a Reynolds number $Re = U_{scale}\, h_{log}\, \nu^{-1} \sim 10^4$, where $h_{log} \sim 10^{-1}$ m is the thickness of the logarithmic layer and $\nu = 1.6 \times 10^{-6}\,m^2\,s^{-1}$, is the kinematic viscosity. This suggests a transitional flow regime between viscous and turbulent [*Monin and Yaglom*, 1965]. Slight deflection of the velocity vector to the left when approaching the lake bottom suggests this boundary layer is affected by the Coriolis force. From law of the wall [*Monin and Yaglom*, 1965], the mean eddy viscosity within the logarithmic layer can be estimated as $K_Z = 1/2\ u_*\ h_{log} \kappa^{-1} \sim 10^{-4}\,m^2\,s^{-1}$, $\kappa = 0.4$ is the von Karman constant. Using this estimate of K_Z gives a scale for the thickness of the Ekman boundary layer of $h_f = (K_Z\, f^{-1})^{1/2} = (u_*\, h_{log})^{1/2} (\kappa\, f)^{-1/2} \sim 1$ m, where $f \sim 10^{-4}\,s^{-1}$ is the inertial frequency at the lake's latitude. The observed current rotates in a layer of similar thickness of 1–2 m (Figure 2c); however, the rotation is much weaker than expected for a Coriolis-friction balance [*Gill*, 1982]. Hence, the negatively buoyant plume appears balanced primarily by the viscosity in its lower 0.5 m and by the entrainment into the ambient lake water at its top.

4.3. Entrainment

If the observed bottom density flow is in steady state equilibrium with the ambient fluid, the rate of its entrainment, E, into the lake water is determined by the Richardson number of the flow $Ri = (\Delta b\, h_{down})\ u_{down}^{-2} \approx 0.55$ as [*Turner*, 1986] $E = (0.08 - 0.1\,Ri)(1 + 5Ri)^{-1} \approx 6 \times 10^{-3}$. Here $\Delta b = 0.5 \times 10^{-4}\,m\,s^{-2}$ is the buoyancy difference between the density flow and the overlying lake waters (Figure 2a). The in situ entrainment rate, $E = (dh_{down})(dx)^{-1}$, can be directly estimated from relative slopes of the lake bottom and the upper boundary of the downslope flow detected from isolines of constant buoyancy (temperature) [e.g., *Forrest et al.*, 2012] as $E \approx 2$–$5\,m\,km^{-1} \approx 3.5 \times 10^{-3}$. The good agreement between both estimates of E validates the assumption of steady state. These estimates of E are also consistent with observations by *Stefanovic and Stefan* [2002] who obtained a value of 8×10^{-3} for density currents in an ice-covered lake. Entrainment can also be expressed as the ratio of underflow to vertical velocity, $E = w_e\ u_{down}^{-1}$ [*Ellison and Turner*, 1959]. Our estimate of E from 3.5×10^{-3} to 6×10^{-3} indicates w_e is 3 orders of magnitude smaller than u_{down}, suggestive of the convective motion being driven by marginal buoyancy flux is predominantly a horizontal exchange between the nearshore and pelagic regions.

4.4. Continuity

The steady state bottom density flow converging to the lake center requires an overlying, compensating shoreward flow to exist. Indeed, slow shoreward flow at speeds $u_{back} \approx 5 \times 10^{-3}\,m\,s^{-1}$ are present above the downslope boundary current (Figure 2b). For steady state axisymmetric circulation, continuity requires $Q_{under} = u_{down} \times h_{down} \approx u_{back} \times (H\text{-}h_{down}) = Q_{back}$ to be valid at any horizontal location in the lake, where Q_{under} and Q_{back} are the depth integrated flows per unit width in the lower and upper layer, respectively, and H is the lake depth at this location. Adopting the previously established values for u_{down}, h_{down}, and u_{back}, one finds that for the measured velocity profiles $Q_{under} \approx Q_{back} \sim 10^{-1}\,m^2\,s^{-1}$. That is, the depth-integrated radial volume transport is in a local balance, which further supports the steady state lake-wide character of the observed mean circulation.

The width of the central upwelling zone associated with the steady state circulation described above is observed to be comparable to the internal Rossby radius of deformation $R = cf^{-1}$ [*Forrest et al.*, 2013], where $c = (g'h)^{1/2}$ is the internal wave speed for water depth h, and $g' = (g\Delta\rho)\rho_0^{-1} = \Delta b$ the reduced gravity based on the buoyancy difference between the upwelling area and surrounding water. Estimating

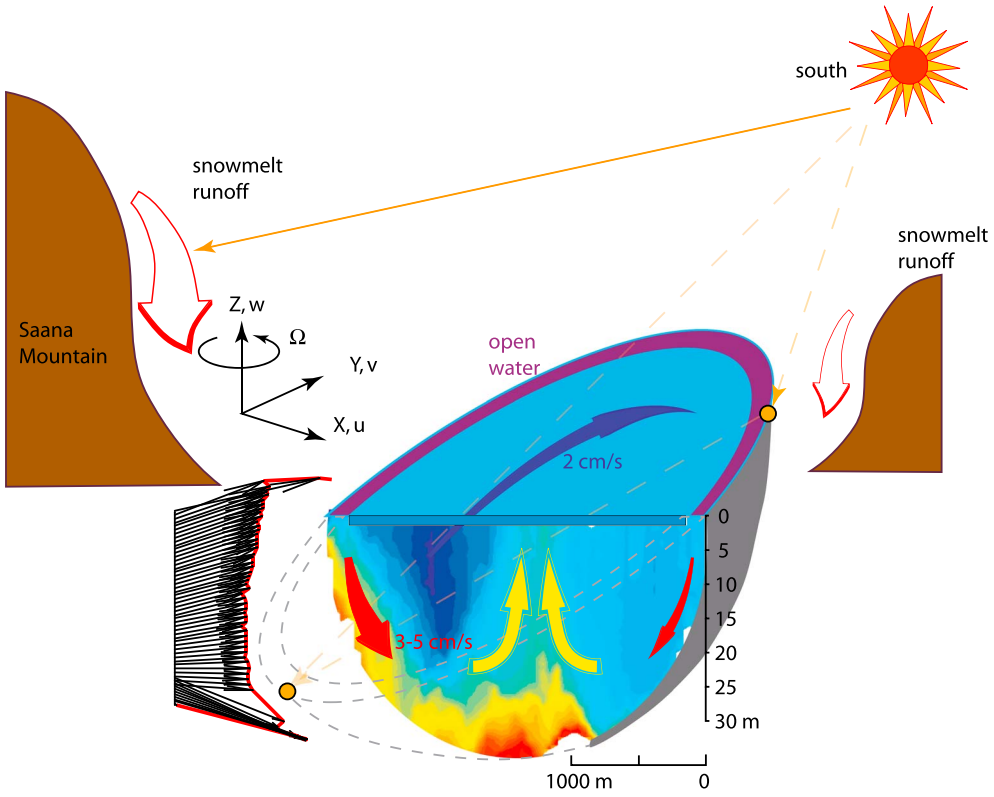

Figure 3. Conceptual drawing showing the axisymmetric circulation pattern along with the main driving forces.

$\Delta b = 0.5 \times 10^{-4}\,\mathrm{m\,s^{-2}}$ (Figure 2a) and using the depth of the base of the upwelling $h \approx 20\,\mathrm{m}$, gives $R = 300\,\mathrm{m}$, which compares well with the observed radius of the upwelling of about 300 m (Figure 2b). Using R as characteristic length scale of the upwelling, the upward velocity in the upwelling zone w_u can be estimated from continuity considerations $u_{\mathrm{down}} \times h_{\mathrm{down}} \sim w_u \times R$ as $w_u \sim 10^{-4}\,\mathrm{m\,s^{-1}}$.

4.5. Anticyclonic Longshore Circulation

The relatively strong anticyclonic longshore current ($u_{\mathrm{theta}} \sim 2\,\mathrm{cm\,s^{-1}}$) occupying the bulk of the water column is an intriguing feature of the observed circulation pattern. To reveal its origin, we note the downslope boundary layer flow requires a compensating flow in the shoreward direction, and this compensating flow develops in the weakly stratified bulk of the water column away from the boundary layers and therefore experiences low friction and no appreciable baroclinic pressure gradients. Therefore, within this compensating flow, the only mechanism balancing local flow acceleration in the shoreward direction is the Coriolis force, whose importance is predicted by a small Rossby number $u_{\mathrm{back}} L^{-1} f^{-1} \sim 10^{-1}$, where $L \sim 10^3\,\mathrm{m}$ is the lateral scale of the flow and $u_{\mathrm{back}} \sim 10^{-2}\,\mathrm{m\,s^{-1}}$. Hence, the shoreward compensating flow at its initial stage is nearly inertial, i.e., it rotates *anticyclonically* with the local inertial period $T_f = 2\pi f^{-1} \approx 12.7\,\mathrm{h}$. In order to turn into a longshore jet, the compensating flow should be balanced by a normal-to-shore force. The radial baroclinic pressure gradient is one candidate to be a balancing force. The upwelling in the center creates an offshore baroclinic pressure gradient (1500–1750 m from the southwest shore in Figures 1d and 2a) of the order $(\partial b)(\partial x)^{-1} \approx (4.75 - 4.50) \times 10^{-4}\,\mathrm{m\,s^{-2}}/250\,\mathrm{m} \sim 10^{-7}\,\mathrm{s^{-2}}$. An upper scale estimation for the anticyclonic longshore velocity created by this gradient and balanced by the Coriolis force follows from the simple geostrophic balance $(H\text{-}h_{\mathrm{down}}) f^{-1} (\partial b)(\partial x)^{-1} \sim 10^{-2}\,\mathrm{m\,s^{-1}}$, which is comparable to the measured longshore current of $u_{\mathrm{theta}} = 2\text{–}4\,\mathrm{cm\,s^{-1}}$. However, the density gradient in the central part of the lake is counterbalanced by the density gradient of opposite direction in the nearshore area (2000–2750 m along the x axis in Figure 2b), which should slow down the anticyclonic flow. A key factor entering the balance of forces in this situation is the bottom slope. The pressure gradient force along the direction of the bottom slope $(\partial P)(\partial x)^{-1}$ includes a term of $-g(\partial h)(\partial x)^{-1}$ directed toward the shallow areas, which adjusts the

Coriolis-balanced flow along isobaths and additionally intensifies the anticyclonic rotation. In this sense, our observations reproduce closely the effect of "hypsography" production of zonal anticyclonic current, described by *Condie and Rhines* [1994a, see also *Rhines*, 1998] based on laboratory experiments in a rotating bowl-shaped basin with buoyancy sink at the surface.

In summary of the analysis above, it can be stated that the observed, nearly steady state anticyclonic circulation is driven by the density gradient at the outer edge of the midlake upwelling area and the bottom slope at the other side (Figure 3) and balanced by the Earth's rotation.

5. Discussion

Heat input along the lateral margins from meltwater runoff and/or differential heating of moat water is a common feature of polar lakes produced by a large amount of solar radiation in the polar summer and by the strong albedo difference between the highly reflective ice surface and surroundings. In areas with low precipitation rates, like Antarctic proglacial lakes such as Lake Vanda, regular appearance of moats in summer have also been reported [*Spigel and Priscu*, 1998; *McKay et al.*, 2005], suggesting similar marginal buoyancy forcing could potentially exist there. Similar circulation patterns, but of smaller magnitudes, can be implied to exist in subglacial lakes isolated from solar heating: contemporary conceptual models of Lake Vostok circulation [*Wüest and Carmack*, 2000; *Williams*, 2001] suggest marginal production of negative buoyancy flux through friction forces and by melting of the glacier ceiling over the lake. In temperate ice-covered lakes this circulation mechanism is probably of less importance, as the marginal heating is generally weaker as a result of smaller incoming radiation and the greater diurnal cycle of solar heating.

Rotating gravity flow over a sloping boundary is a classical problem of fluid dynamics with many applications in oceanic and atmospheric sciences. Our observations in an ice-covered lake, having constant temperature at the surface and effectively isolated from momentum sources at the surface (except oscillations of the ice cover), provide a quantitative insight in characteristics of these natural flows, available otherwise only from laboratory simulations. Among these results is evidence of the "hypsographic effect" mentioned above, i.e., intensification of zonal anticyclonic current by the bottom slope in a rotating bowl-shaped basin with a buoyancy sink at the surface. Laboratory experiments of *Condie and Rhines* [1994a] demonstrated that this effect produces so-called "topographic Hadley cells"—two-cell radial circulation identical to that described here. Its importance can be further emphasized recalling the analogy between the bottom slope and the variation of the Coriolis force with latitude that makes the observed circulation similar to global circulation of convectively driven atmospheres (e.g., zonal flow production in atmospheres of Jupiter and Saturn) [*Condie and Rhines*, 1994b].

A distinct feature of circulation driven by lateral buoyancy forcing at the lake periphery, as reported in this work, is that it occupies the entire lake body and will result in both transport of dissolved matter and algae cells from the deep waters to the euphotic layer by the central upwelling and oxygenation of the benthic water layers by downslope gravity currents. The former effect can play a crucial role in the transport of nutrients accumulated in sediments to the upper water layers and the genesis of the spring algae bloom of diatoms, the dominating algae species in ice-covered lakes. These organisms require some additional mechanism to maintain their buoyancy in the upper layers [*Kelley*, 1997; *Jewson et al.*, 2010]. The latter effect of the oxygen supply to the deep waters is important in eutrophic lakes, where deep water anoxia is created under ice by anaerobic bacteria activity due to isolation from the atmosphere and low rates of vertical mixing [*Golosov et al.*, 2007, 2012; *Terzhevik et al.*, 2009]. Hence, the vertical circulation cells established in this type of circulation (Figure 3) maintain the important link between the deep and shallow parts of the lake ecosystem, whereas the anticyclonic longshore jet ensures equal redistribution of the meltwater-driven effects over the entire lake.

Acknowledgments

This study was performed in frames of the EU FP7 Program "International Network for Terrestrial Research and Monitoring in the Arctic (INTERACT)" via transnational access projects "Convection and currents under lake ice (CONCUR) 2013" and "Lake circulation during polar night in Arctic (LACUNA 2014)." We thank the personnel of the Kilpisjärvi Biological Station and the rest of our field team for their invaluable help with our field campaigns. In particular, we are indebted to Antero Järvinen, the Station Director, for his continued support. G.K. was partially supported by the German Science Foundation (grant KI-853/6). K.G. was partially supported by the Canadian Northern Science Training Program. K.G. and B.L. were partially supported by the Canadian Natural Sciences and Engineering Research Council Discovery program. We thank two anonymous reviewers for constructive comments improving original version of this work. Arrays of CTD and current meter data behind Figures 1 and 2 are stored in the internal repository of the IGB Berlin and are available from the corresponding author by first request.

The Editor thanks two anonymous reviewers for their assistance in evaluating this paper.

References

Chen, C.-T. A., and F. J. Millero (1986), Precise thermodynamic properties for natural waters covering only the limnological range, *Limnol. Oceanogr.*, *31*(3), 657–662, doi:10.4319/lo.1986.31.3.0657.

Condie, S. A., and P. B. Rhines (1994a), Topographic Hadley cells, *J. Fluid Mech.*, *280*, 349–368.

Condie, S. A., and P. B. Rhines (1994b), A convective model for the zonal jets in the atmospheres of Jupiter and Saturn, *Nature*, *367*(6465), 711–713.

Ellison, T. H., and J. S. Turner (1959), Turbulent entrainment in stratified flows, *J. Fluid Mech.*, *6*(03), 423–448.

Farmer, D. M. (1975), Penetrative convection in the absence of mean shear, *Q. J. R. Meteorol. Soc.*, *101*(430), 869–891, doi:10.1002/qj.49710143011.
Forrest, A. L., B. E. Laval, R. Pieters, and D. S. Lim (2008), Convectively driven transport in temperate lakes, *Limnol. Oceanogr.*, *53*(5), 2321–2332, doi:10.4319/lo.2008.53.5_part_2.2321.
Forrest, A. L., H. Ó. Andradóttir, and B. E. Laval (2012), Preconditioning of an underflow during ice-breakup in a subarctic lake, *Aquat. Sci.*, *74*(2), 361–374, doi:10.1007/s00027-011-0227-2.
Forrest, A. L., B. E. Laval, R. Pieters, and D. S. S. Lim (2013), A cyclonic gyre in an ice-covered lake, *Limnol. Oceanogr.*, *58*(1), 363–375, doi:10.4319/lo.2013.58.1.0363.
Gill, A. E. (1982), *Atmosphere Ocean Dynamics*, 662 pp., Academic Press, San Diego, Calif.
Golosov, S., O. Maher, E. Schipunova, A. Terzhevik, G. Zdorovennova, and G. Kirillin (2007), Physical background of the development of oxygen depletion in ice-covered lakes, *Oecologia*, *151*(2), 331–340.
Golosov, S., A. Terzhevik, I. Zverev, G. Kirillin, and C. Engelhardt (2012), Climate change impact on thermal and oxygen regime of shallow lakes, *Tellus, Ser. A*, *64*, 17,264, doi:10.3402/tellusa.v64i0.17264.
Huttula, T., M. Pulkkanen, B. Arkhipov, M. Leppäranta, V. Solbakov, K. Shirasawa, and K. Salonen (2010), Modelling circulation in an ice-covered lake, *Est. J. Earth Sci.*, *59*(4), 298, doi:10.3176/earth.2010.4.06.
Jewson, D. H., N. G. Granin, A. A. Zhdarnov, L. A. Gorbunova, and R. Y. Gnatovsky (2010), Vertical mixing, size change and resting stage formation of the planktonic diatom *Aulacoseira baicalensis*, *Eur. J. Phycol.*, *45*(4), 354–364.
Kelley, D. E. (1997), Convection in ice-covered lakes: Effects on algal suspension, *J. Plankton Res.*, *19*(12), 1859–1880.
Kirillin, G., and A. Terzhevik (2011), Thermal instability in freshwater lakes under ice: Effect of salt gradients or solar radiation?, *Cold Reg. Sci. Technol.*, *65*(2), 184–190, doi:10.1016/j.coldregions.2010.08.010.
Kirillin, G., et al. (2012), Physics of seasonally ice-covered lakes: A review, *Aquat. Sci.*, *74*(4), 659–682, doi:10.1007/s00027-012-0279-y.
Lei, R., M. Leppäranta, B. Cheng, P. Heil, and Z. Li (2012), Changes in ice-season characteristics of a European Arctic lake from 1964 to 2008, *Clim. Change*, *115*(3-4), 725–739.
McKay, C. P., D. T. Andersen, W. H. Pollard, J. L. Heldmann, P. T. Doran, C. H. Fritsen, and J. C. Priscu (2005), Polar lakes, streams, and springs as analogs for the hydrological cycle on Mars, in *Water on Mars and Life*, pp. 219–233, Springer, Berlin, Heidelberg.
Mironov, D., A. Terzhevik, G. Kirillin, T. Jonas, J. Malm, and D. Farmer (2002), Radiatively-driven convection in ice-covered lakes: Observations, scaling and mixed-layer model, *J. Geophys. Res.*, *107*(C4), 3032, doi:10.1029/2001JC000892.
Monin, A. S., and A. M. Yaglom (1965), *Statistical Fluid Mechanics: Mechanics of Turbulence*, vol. 1, Dover Publ., New York.
Nolan, M., G. Liston, P. Prokein, J. Brigham-Grette, V. L. Sharpton, and R. Huntzinger (2002), Analysis of lake ice dynamics and morphology on Lake El'gygytgyn, NE Siberia, using synthetic aperture radar (SAR) and Landsat, *J. Geophys. Res.*, *107*(D2), 8162, doi:10.1029/2001JD000934.
Rhines, P. B. (1993), Oceanic general circulation: Wave and advection dynamics, in *Modelling Oceanic Climate Interactions*, pp. 67–149, Springer, Berlin, Heidelberg.
Rhines, P. B. (1998), Circulation, convection and mixing in rotating, stratified basins with sloping topography, in *Physical Processes in Lakes and Oceans*, *Coastal and Estuarine Studies*, vol. 4, edited by J. Imberger, pp. 209–226, AGU, Washington, D. C., doi:10.1029/CE054p0209.
Rizk, W., G. Kirillin, and M. Leppäranta (2014), Basin-scale circulation and heat fluxes in ice-covered lakes, *Limnol. Oceanogr.*, *59*(2), 445–464.
Salonen, K., M. Pulkkanen, P. Salmi, and R. W. Griffiths (2014), Interannual variability of circulation under spring ice in a boreal lake, *Limnol. Oceanogr.*, *59*(6), 2121–2132, doi:10.4319/lo.2014.59.6.2121.
Siegert, M. J. (2005), Lakes beneath the ice sheet: The occurrence, analysis, and future exploration of Lake Vostok and other Antarctic subglacial lakes, *Annu. Rev. Earth Planet. Sci.*, *33*, 215–245.
Spigel, R. H., and J. C. Priscu (1998), Physical limnology of the McMurdo Dry Valleys lakes, in *Ecosystem Dynamics in a Polar Desert: The Mcmurdo Dry Valleys, Antarctica*, pp. 153–187, AGU, Washington, D. C.
Stefanovic, D. L., and H. G. Stefan (2002), Two-dimensional temperature and dissolved oxygen dynamics in the littoral region of an ice-covered lake, *Cold Reg. Sci. Technol.*, *34*(3), 159–178, doi:10.1016/S0165-232X(02)00003-4.
Terzhevik, A., S. Golosov, N. Palshin, A. Mitrokhov, R. Zdorovennov, G. Zdorovennova, G. Kirillin, E. Shipunova, and I. Zverev (2009), Some features of the thermal and dissolved oxygen structure in boreal, shallow ice-covered Lake Vendyurskoe, Russia, *Aquat. Ecol.*, *43*(3), 617–627, doi:10.1007/s10452-009-9288-x.
Turner, J. S. (1986), Turbulent entrainment: The development of the entrainment assumption, and its application to geophysical flows, *J. Fluid Mech.*, *173*, 431–471, doi:10.1017/S0022112086001222.
Williams, M. J. (2001), Application of a three-dimensional numerical model to Lake Vostok: An Antarctic subglacial lake, *Geophys. Res. Lett.*, *28*(3), 531–534, doi:10.1029/2000GL012107.
Wüest, A., and E. Carmack (2000), A priori estimates of mixing and circulation in the hard-to-reach water body of Lake Vostok, *Ocean Modell.*, *2*(1), 29–43.